JOURNAL OF SOLID STATE CHEMISTRY 56, 84–93 (1985)

Defect Structures in the Brannerite-Type Vanadates

VI. Preparation and Study of $Co_{1-x}\phi_xV_{2-2x}Mo_{2x}O_6$ and Phase Diagram of the Ternary $CoO–V_2O_5–MoO_3$ System

KRZYSZTOF MOCAŁA, JACEK ZIÓŁKOWSKI,* AND LIDIA DZIEMBAJ

Institute of Catalysis and Surface Chemistry, Polish Academy of Sciences, 30-239 Kraków, ul. Niezapominajek, Poland

Received February 24, 1984; in revised form June 11, 1984

The phase diagram of the ternary $CoO–V_2O_5–MoO_3$ system and in particular its $T–CoV_2O_6–MoO_3$ slice have been determined with DTA and X-ray phase analysis. CoV_2O_6 crystallizes in two modifications: a low-temperature γ-form of unknown structure and a high-temperature α-form of brannerite-type structure. The transition temperature is 660–665°C. The $\gamma \rightleftarrows \alpha$ transformations are very slow and the α-polymorph may be easily frozen. On doping with MoO_3, a solid solution is formed that is described by the formula $Co_{1-x}\phi_xV_{2-2x}Mo_{2x}O_6$. Above $x = 0.02$ the α-type structure is stabilized. The x_{max} equals 0.22 at the eutectic temperature of 620°C and 0.20 at room temperature. Other features of the phase diagram, including its division into the natural subdiagrams and three ternary eutectics, are described in detail. X-Ray data are listed for α-CoV_2O_6 and for the solid solution having $x = 0.20$. On doping with MoO_3 the monoclinic lattice dilates primarily in the direction of the b-axis.

Introduction

In the present series of investigations (*1–5*) we have focused our attention on the solid solutions of MoO_3 in the matrices of metal vanadates AV_2O_6 crystallizing in the brannerite-type structure, Fig. 1 (*1, 6, 7*). Previously we have found solid solutions described by the formulas: $Mn_{1-x}\phi_xV_{2-2x}Mo_{2x}O_6$ ($0 \le x \le 0.45$) (*1, 2, 4*); $Mn_{1-x-y}\phi_xLi_yV_{2-2x-y}Mo_{2x+y}O_6$ ($0 \le x \le 0.45$; $0 \le y \le 1$) (*5*); $Cu^{2+}_{1-x-y}\phi_xCu^{1+}_yV_{2-2x-y}Mo_{2x+y}O_6$ ($0 \le x \le 0.23$; $0 \le y \le 0.27$) (*3*); and we have mentioned that solutions analogous to $Mn_{1-x}\phi_xV_{2-2x}Mo_{2x}O_6$ are also formed in the $CoV_2O_6–MoO_3$ and $ZnV_2O_6–MoO_3$ systems (*1*). In these solutions Mo^{6+} ions are substituted at random for V^{5+} ions and charge compensation is accomplished either by an equivalent number of cationic vacancies ϕ at bivalent metal sites, by partial reduction of the bivalent metal, or by replacing it with a Li^{1+} ion; A^{2+}, A^{1+}, Li^{1+}, and ϕ being distributed statistically in positions A. On the other hand, Galy and Darriet (*8, 9*) have shown that position A in the brannerite-type matrix may be entirely filled up with typically monovalent cations ($LVMoO_6$) and that an increase of the Mo^{6+}/V^{5+} ratio results in a deficiency of monovalent cation ($L_{1-x}\phi_xV_{1-x}Mo_{1+x}O_6$, L = Li, $0 \le x \le 0.16$; L = Na, $0 \le x \le 0.30$; L = K, $0.18 \le x \le 0.24$; L = Ag, $0 \le x \le 0.12$).

We believe that collecting a number of data concerning the multicomponent oxide

* To whom all correspondence should be addressed.

0022-4596/85 $3.00

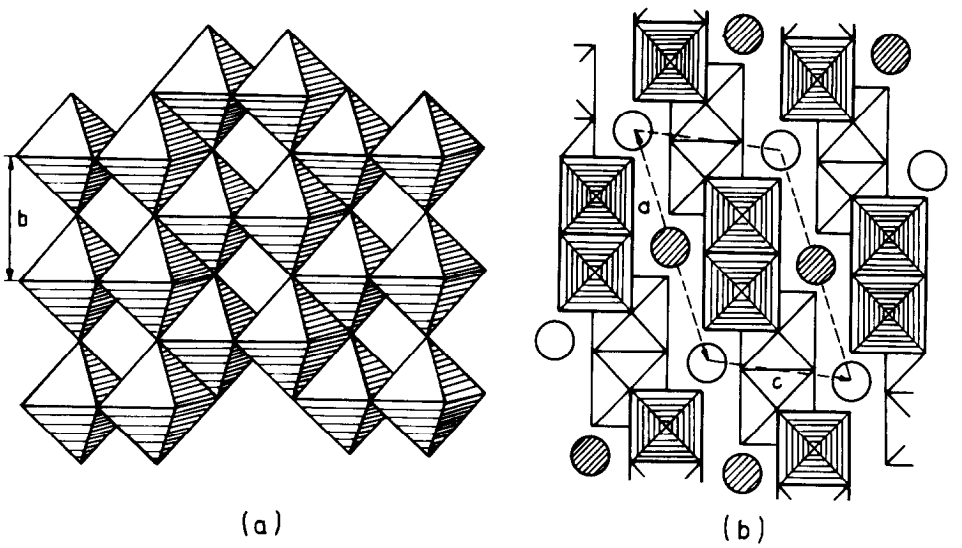

FIG. 1. Idealized outline of the brannerite-type AV_2O_6 structure (after (6)). (a) A sheet of VO_6 octahedra parallel to (001) plane; (b) projection of the structure on the *ac* plane with marked *A* cations at two different levels.

solid solutions of the oxysalt-type matrix will bring us closer to understanding the laws governing their formation. Moreover, the studied solutions exhibit some interesting catalytic properties including the effect of catalytic anisotropy (*10–13*). Therefore, in the present paper our studies are extended onto the $CoO-V_2O_5-MoO_3$ system comprising $Co_{1-x}\phi_xV_{2-2x}Mo_{2x}O_6$ solid solution, which will be labeled throughout the paper as Coϕ-*X* ($X = 100x$) or briefly as Coϕ if the indication of composition is not necessary. The composition of Coϕ may be expressed as $Co_{1-x}\phi_xV_{2-2x}Mo_{2x}O_6$ or $(1 - x)CoV_2O_6 + 2xMoO_3$ which indicates that this solution is localized along the CoV_2O_6–MoO_3 section of the $CoO-V_2O_5-MoO_3$ diagram.

According to literature data CoV_2O_6 crystallizes in two modifications: a γ-form of an unknown structure, but of a known X-ray pattern (*14*) and an α-form of brannerite-type structure (*15*) with the transition temperature of 662°C (*16*). In this paper we shall provide some further information in this respect. It will be shown that γ and α are the low-temperature and high-temperature polymorphs, respectively, but doping with MoO_3 stabilizes the brannerite-type modification.

Experimental

The way of preparing Coϕ solid solutions has been elaborated empirically with the method of trials. Weighed quantities of $CoCO_3 \cdot nH_2O$, $(NH_4)_6Mo_7O_{24} \cdot 4H_2O$ and "active" V_2O_5 (freshly precipitated from an aqueous solution of NH_4VO_3 with HNO_3, dried at 120°C for 20 hr and annealed at 500°C for 20 hr) were ground and preheated in quartz tubes at 615°C for 15 min to remove the volatiles. After grinding they were calcined as shown in Table I. X-Ray analysis showed the formation of pure CoV_2O_6 or Coϕ solid solutions for samples of $X < 20$. The samples of higher content of

TABLE I

EXPERIMENTAL CONDITIONS FOR PREPARATION OF SAMPLES ALONG CoV_2O_6–MoO_3 SECTION (STARTING MATERIALS: $CoCO_3 \cdot nH_2O$, $(NH_4)_6Mo_7O_{24} \cdot 4H_2O$, "Active" V_2O_5)

x	Calcination conditions	Phase composition
0	720°C/45 hr and quenching	α-CoV_2O_6
0	600°C/40 hr	γ-CoV_2O_6
0.002 0.005 0.01	620°C/20 hr + 640°C/40 hr	α-Coϕ + γ-CoV_2O_6
0.02	*T*	α-Coϕ
0.04	*T*	α-Coϕ
0.06	*T*	α-Coϕ
0.08	*T*	α-Coϕ
0.10	*T*	α-Coϕ
0.12	*T*	α-Coϕ
0.14	*T*	α-Coϕ
0.16	*T*	α-Coϕ
0.18	*T*	α-Coϕ
0.20	*T*	α-Coϕ + traces of a,b-$CoMoO_4$, *VM*
0.22	*T*	α-Coϕ + a,b-$CoMoO_4$ + *VM*
0.24	*T*	α-Coϕ + a,b-$CoMoO_4$ + *VM*
0.26	*T*	α-Coϕ + a,b-$CoMoO_4$ + *VM*
0.28	*T*	α-Coϕ + a,b-$CoMoO_4$ + *VM*
0.30	*T*	α-Coϕ + a,b-$CoMoO_4$ + *VM*
0.33	*Q*	α-Coϕ + a,b-$CoMoO_4$ + *VM*
0.36	*T*	α-Coϕ + a,b-$CoMoO_4$ + *VM*
0.40	S_1	a,b-$CoMoO_4$ + *VM* + traces of V_2MoO_8
0.46	S_1	a,b-$CoMoO_4$ + *VM* + V_2MoO_8
0.50	S_1	a,b-$CoMoO_4$ + V_2MoO_8 + traces of *VM* and MoO_3
0.54	S_1	a,b-$CoMoO_4$ + V_2MoO_8 + traces of MoO_3
0.60	S_2	a,b-$CoMoO_4$ + V_2MoO_8 + MoO_3
0.64	S_2	a,b-$CoMoO_4$ + V_2MoO_8 + MoO_3
0.70	S_2	a,b-$CoMoO_4$ + V_2MoO_8 + MoO_3
0.80	S_2	a,b-$CoMoO_4$ + V_2MoO_8 + MoO_3
0.92	S_2	a,b-$CoMoO_4$ + V_2MoO_8 + MoO_3

Note. *VM* = $V^{5+}_{2-y}V^{4+}_yMo^{6+}_yO_5$ solid solution; *T* = 610°C/45 hr; *Q* = Mixture of $CoMoO_4$ and V_2O_5 (1 : 1) heated at 630°C for 20 hr and slowly (1,5°C/hr) cooled to 570°C; S_1 = Stepwise calcination 550°C/30 hr + 570°C/75 hr + 600°C/72 hr + 605°C/44 hr; S_2 = Stepwise calcination 570°C/45 hr + 580°C/72 hr + 600°C/70 hr.

MoO_3 and lying along the CoV_2O_6–MoO_3 section exhibited the presence of a-$CoMoO_4$, b-$CoMoO_4$, V_2MoO_8, MoO_3, and a solid solution of MoO_3 in V_2O_5 (labeled as *VM*) which is believe to be described by the formula $V^{5+}_{2-2y}V^{4+}_yMo^{6+}_yO_5$ (*17*) (Table I). To be sure that the last-mentioned multiphase preparations had already reached the equilibrium state they were annealed again at the respective temperatures for some scores of hours but no change in their phase composition was observed with the exception of the ratio between a- and b-$CoMoO_4$. As it is known the transition temperature between a low-temperature b-$CoMoO_4$ and a high-temperature a-$CoMoO_4$ is about 410°C (*18–20*), but the a → b transformation is hindered at lower temperatures and depends on the intensity of grinding and other biographical factors (*21–24*). A number of preparations of composition lying outside the CoV_2O_6–MoO_3 section (marked in Fig. 3) were prepared by mixing the same starting materials as indicated above or $CoMoO_4 + V_2O_5$, $CoMoO_4$ + α-Coϕ-20, and $CoMoO_4$ + α-CoV_2O_6 then heating these mixtures for 100 hr just below the solidus (570–730°C) as determined with DTA. $CoMoO_4$ was synthesized as described in (*22*).

The X-ray diffraction patterns were obtained with a DRON-2 diffractometer using Cr radiation and an internal standard of Al $a = 4.0492$ Å at 25°C. Phase identification was based upon published patterns (*14, 25, 26*). V_2O_5 and *VM* were distinguished by a shift of the (400) and (110) lines, consistent with the changes in lattice parameters reported in (*17*). Our X-ray pattern of α-CoV_2O_6 differed to some extent from that published by Sauerbrei (*15*). We have therefore redetermined its lattice parameters, and we have determined those for Coϕ solid solutions, at room temperature, using 12–18 reflections of $2\theta \geq 59°$ and applying the least-squares method (cf. Tables II and III and Fig. 2).

Elemental analysis (Pye–Unicam FP 90 spectrometer), DTA (SETARAM M5 microanalyzer, 10°/min, Pt crucibles, samples of 12.5 mg) and the treatment of DTA curves were performed in the same way as was described in the previous paper (*5*).

EPR spectra were recorded in an X-band at room temperature using an EPR spectrometer of Wrocław Polytechnic.

Results and Discussion

(I) Phase Transformations of CoV_2O_6 and of Coϕ Solid Solutions

The low-temperature γ-CoV_2O_6 may be obtained by annealing the stoichiometric mixture of $CoCO_3 \cdot nH_2O$ and "active" V_2O_5 at 600°C for 40 hr, while the high-temperature brannerite-type α-CoV_2O_6 may be synthesized by heating an analogous mixture at 720°C for 45 hr followed by air quenching to room temperature. Phase transformation is very slow and no DTA peak was observed. γ-CoV_2O_6 transforms entirely to α-CoV_2O_6 after heating at 730°C for a few hours, while at 700°C even after 100 hr only a partial $\gamma \rightarrow \alpha$ transformation was observed. Total $\alpha \rightarrow \gamma$ transition requires heating the α-form at 660°C for 20 hr.

A number of samples of α- and γ-forms were submitted to prolonged heating at 660–700°C, quenching, and X-ray phase analysis. On this basis the transition temperature was found to be between 660 and 665°C which agrees excellently with Clark and Pick's result (*16*) they, however, did not indicate which is the high temperature, and which is the low temperature polymorph.

All samples of Coϕ solid solutions of $2 < X < 20$ exhibited the α-type structure and no phase transformation was observed either on cooling or on heating with various temperature programs. Coϕ samples of X equal to 0.2, 0.5, and 1 contained the α-phase more or less "contaminated" with the γ-phase, the latter disappearing on heating at 730°C. Coϕ-2 after prolonged annealing at 350°C and air quenching conserved the α-type structure. The same preparation when slowly cooled down (1.5°/hr) from 350°C to room temperature with annealing for 20 hr each 50°C, contained a trace of the γ-form. These results enable us to conclude that doping with MoO_3 stabilizes the brannerite-type structure of Coϕ solid solutions. It is only below X = 3 that we find an area of coexistence of γ-CoV_2O_6 and α-Coϕ. However, it cannot be excluded that this area is in fact composed of two subareas: γ-Coϕ (including γ-Coϕ-O = CoV_2O_6) and γ-Coϕ + α-Coϕ.

(II) Verification of the Coϕ Formula

The formula $Co_{1-x}\phi_xV_{2-2x}Mo_{2x}O_6$ has been verified on the basis of elemental analysis, X-ray phase analysis, and EPR spectra. The elemental analysis of samples with $2 < X < 20$, performed after the final thermal treatment has shown a stoichiometry corresponding to the assumed Coϕ formula, within the error of the analytical method (1%). X-Ray phase analysis of these samples has shown that they contain solely the α-type phase with some reflections (especially those of $k \neq 0$) being more and more shifted along the series which proves that solid solutions were formed (see the next paragraph). Let us remark that in principle, charge compensation could be accomplished in other ways, e.g.; $Co^{2+}V^{5+}_{2-2x}V^{4+}_xMo^{6+}_xO_6$ or $Co^{2+}V^{5+}_{2-x}Mo^{5+}_xO_6$, but these hypothetical formulations do not have the correct stoichiometry. If these hypothetical solutions were formed, part of the material should remain as excess phases which should be easily detected with X-ray phase analysis (cf. an analogous discussion in (*5*)).

Let us note, moreover, that without a change in composition Coϕ solid solutions could exhibit a valence isomerism: $Co^{2+}_{1-y}Co^{3+}_yV^{5+}_{2-y}V^{4+}_yO_6$ (for Coϕ-0) and $Co^{2+}_{1-x-y}Co^{3+}_y\phi_xV^{5+}_{2-2x-y}V^{4+}_yMo^{6+}_{2x}O_6$ (for Coϕ-X). Of the three paramagnetic ions, V^{4+} (d^1) is known to give the EPR signal at $g \approx 1.96$ (*17*) while Co^{3+} (d^6) is a non-Kramers-type ion and Co^{2+} (d^7) in octahedron gives no EPR signal at room temperature due to long relaxation time. Our EPR experiments have shown that neither CoV_2O_6 nor α-Coϕ solutions exhibit an EPR spectrum. This excludes the above-mentioned valence isomerism. A signal of the shape and position

corresponding to that reported by Robb *et al.* (*17*) and observed for samples of $20 < X < 40$ may be ascribed to V^{4+} in the *VM* solid solution which was detected in the X-ray analysis of the samples.

(III) X-Ray Studies of α-CoV_2O_6 *and* α-Coϕ

Our X-ray pattern for α-CoV_2O_6, as well as that of α-Coϕ-20, are given in Table II. In

TABLE II

X-RAY POWDER DATA FOR α-CoV_2O_6 AND α-Coϕ-20

CoV_2O_6				$Co_{0.80}\phi_{0.20}V_{1.60}Mo_{0.40}O_6$			
hkl	d_{obs}	d_{cal}	*I*	d_{obs}	d_{cal}	*I*	*hkl*
				6.13	6.12	m	001
$20\bar{1}$	4.35	4.36	s	4.39	4.38	m	$20\bar{1}$
200	4.30	4.30	vw	4.31	4.30	m	200
110	3.243	3.245	s	3.290	3.290	s	110
$20\bar{2}$	3.101	3.100	s	3.109	3.108	s	$20\bar{2}$
002	3.074	3.076	vw	3.090	3.090	m	$11\bar{1}$
$11\bar{1}$	3.052	3.051	s	3.064	3.062	vw	002
201	3.037	3.037	vs	3.025	3.024	vs	201
111	2.718	2.718	s	2.738	2.738	s	111
				2.423	2.422	vw	$11\bar{2}$
$40\bar{1}$	2.312	2.312	vw	2.330	2.329	m	$31\bar{1}$
$31\bar{1}$	2.308	2.308	m	2.322	2.320	m	$40\bar{1}$
310	2.219	2.219	m	2.232	2.233	w	310
$40\bar{2}$	2.179	2.179	w	2.190	2.190	m	$40\bar{2}$
202	2.154	2.154	m	1.151	2.150	w	400
400	2.151	2.150	m	2.142	2.142	m	202
$31\bar{2}$	2.110	2.107	vw	2.125	2.125	w	$31\bar{2}$
112	2.094	2.092	vw	2.096	2.096	vw	112
003	2.050	2.050	s	2.042	2.041	m	003
311	1.919	1.919	m	1.923	1.924	m	311
$40\bar{3}$	1.867	1.867	m	1.874	1.874	m	$40\bar{3}$
$11\bar{3}$	1.853	1.854	m	1.859	1.859	m	$11\bar{3}$
020	1.752	1.752	m	1.780	1.780	m	020
$20\bar{4}$	1.654	1.654	w	1.652	1.652	w	$20\bar{4}$
113	1.634	1.634	m	1.632	1.633	m	113
203	1.632	1.632	m				
$51\bar{1}$	1.630	1.630	vw				
312	1.596	1.596	w	1.595	1.595	m	312
510	1.544	1.544	vw	1.549	1.549	w	510
$22\bar{2}$	1.525	1.525	w	1.543	1.545	w	$22\bar{2}$
022	1.523	1.522	vw	1.534	1.534	w	221
402	1.519	1.519	s	1.531	1.531	w	004
221	1.517	1.518	m	1.512	1.512	m	402
$51\bar{3}$	1.494	1.494	w	1.504	1.504	m	$51\bar{3}$
$31\bar{4}$	1.476	1.476	w	1.481	1.482	w	$31\bar{4}$
600	1.433	1.433	s	1.433	1.433	m	600

TABLE III

CELL PARAMETERS FOR α-CoV_2O_6 AND α-Coϕ-20

α-CoV_2O_6 Sauerbrei (15)		Present work	α-Coϕ-20 Present work
a [Å]	9.18	9.251(2)[a]	9.284(3)
b [Å]	3.55	3.504(1)	3.561(2)
c [Å]	6.64	6.618(2)	6.611(2)
β [deg]	111.08	111.64(1)	112.12(2)
$c \sin \beta$ [Å]	6.20	6.152(2)	6.124(2)
V [Å^3]	201.9	199.39	202.44

[a] Estimated standard deviation.

Table III the lattice parameters of these two samples are listed and compared with those determined by Sauerbrei (*15*). It has been observed that the grains of α-CoV_2O_6 and α-Coϕ orient easily. Therefore we were not able to obtain quantitatively reproducible intensity data even when using a special technique of preparing an unoriented sample (*1*) which was successful with Mn-containing brannerite-type phases.

Lattice parameters for other Coϕ samples of the range $2 < X < 20$ are presented in Fig. 2. As can be seen the increase of X in Coϕ-X from 0 to 20 results in a linear increase of a, b, and V by $\Delta a = 0.36\%$, $\Delta b = 1.57\%$ and $\Delta V = 1.45\%$. The other parameters change in a monotonic but nonlinear manner; $\Delta c = -0.12\%$, $\Delta c \sin \beta = -0.44\%$, $\Delta \beta = 0.43\%$. The changes of a, b, and V can be easily explained taking into account the crystal structure of the brannerite type (Fig. 1) and an analogous discussion performed in (*1, 3, 5*). Formation of Coϕ-X solutions results in substituting the larger Mo^{6+} ion for the smaller V^{5+} (the ionic radii are 0.59 and 0.54 Å, respectively (*27, 28*)). This should primarily give rise to an increase in b, the direction of the tight packing (see (*5*) where the interatomic distances are listed) and should result in a smaller lattice expansion along the a axis where the structure is more loosely packed. The less important and negative changes of c and $c \sin \beta$ are the resultant of two opposite effects consisting in an increase of thickness of $(VO_6)_n$ layers (due to doping with MoO_3)

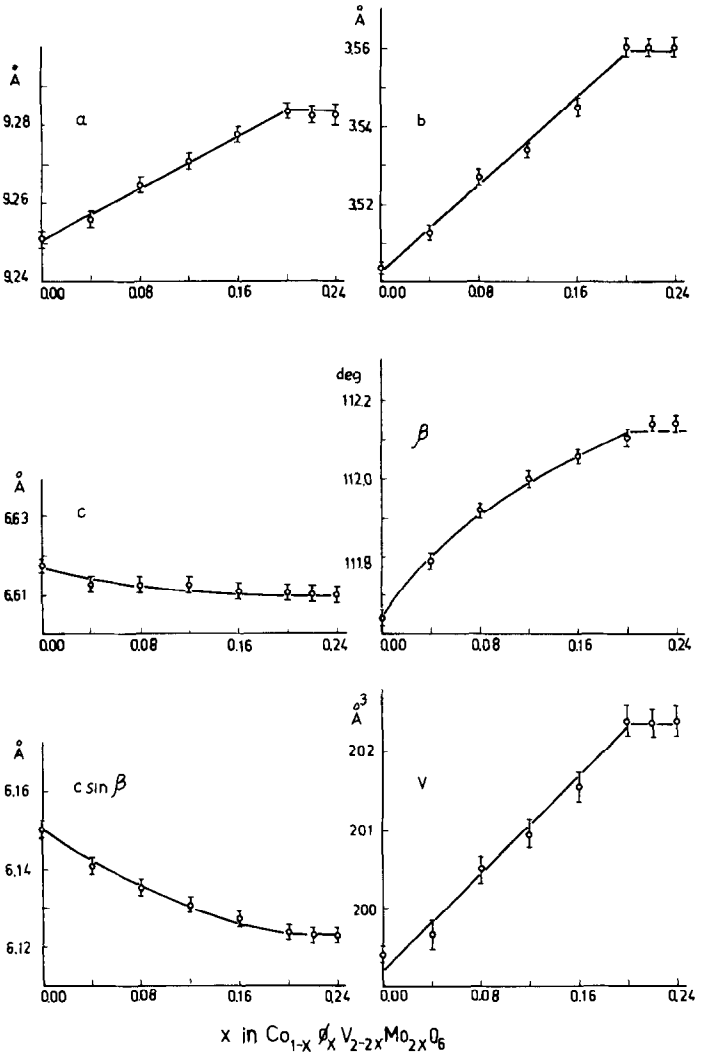

FIG. 2. Cell parameters and cell volume vs x in the $Co_{1-x}\phi_xV_{2-2x}Mo_{2x}O_6$ solid solution.

and a decrease of the distance between these layers produced by the appearance of cation vacancies.

(IV) Phase Diagram

The solid solution $Co\phi = Co_{1-x}\phi_xV_{2-2x}Mo_{2x}O_6$ belongs to the condensed, ternary $CoO-V_2O_5-MoO_3$ system. Its stability range is thus contained in the T–$CoO-V_2O_5-MoO_3$ phase diagram. The composition of $Co\phi$ solution may also be expressed as $(1-x)CoV_2O_6 + 2x\ MoO_3$ which clearly indicates that the stability range of $Co\phi$ must fall in T–$CoV_2O_6-MoO_3$ slice. An analogous situation occurred for $Mn\phi = Mn_{1-x}\phi_xV_{2-2x}Mo_{2x}O_6$ (*1*) where X_{max} was found to be 45. Samples of $45 < X < 100$ were found to be mixtures of MoO_3 and saturated $Mn\phi$-45. This proves that the T–$MnV_2O_6-MoO_3$ slice is the natural binary subdiagram of the ternary T–$MnO-V_2O_5-MoO_3$ diagram (*5*) (except above 760°C). X-Ray phase analysis (Table I) indicates that this is not the case with T–$CoV_2O_6-MoO_3$ and T–$CoO-V_2O_5-MoO_3$ diagrams. Along

CoV_2O_6–MoO_3 and above X_{max}, three ranges may be distinguished: Coϕ-X_{max} + $CoMoO_4$ + *VM*, $CoMoO_4$ + *VM* + V_2MoO_8, and $CoMoO_4$ + V_2MoO_8 + MoO_3 coexist in the subsolidus range. This allowed us to recognize the way of dividing the *T*–CoO–V_2O_5–MoO_3 diagram into the natural subdiagrams as shown in Fig. 3. Three other subareas Coϕ + $CoMoO_4$, Coϕ-X_{max} + *VM*, and Coϕ + V_2O_5 were identified from X-ray analysis.

Namely, as we have indicated in the Introduction and in paragraph (III), the composition of Coϕ (including pure CoV_2O_6) and *VM* (including V_2O_5) may be easily recognized from the shift of the X-ray reflections. The area CoV_2O_6–$CoMoO_4$–CoO is not discussed in this paper in detail.

In view of the above remarks it is clear that *T*–CoV_2O_6–MoO_3 is an arbitrary slice of *T*–CoO–V_2O_5–MoO_3. The composition of the phases coexisting along the CoV_2O_6–MoO_3 section cannot be expressed on this composition scale as the respective tie-lines pierce the plane *T*–CoV_2O_6–MoO_3. It is impossible to understand the equilibria along CoV_2O_6–MoO_3 without some knowledge of the *T*–CoO–V_2O_5–MoO_3 phase diagram. The structures of the last-mentioned ternary diagram and its *T*–CoV_2O_6–MoO_3 slice (Figs. 3–6) were thus determined by using our own X-ray and DTA results and literature data concerning *T*–CoO–MoO_3, *T*–CoO–V_2O_5, and *T*–V_2O_5–MoO_3 external walls. In cases of controversy in the literature data we have verified the key points (e.g., eutectic temperatures) and we have chosen the diagrams which are most consistent with our results.

The *T*–CoO–MoO_3 phase diagram has been determined by Yanushkevitch *et al.* (*20*). There is one compound in this system,

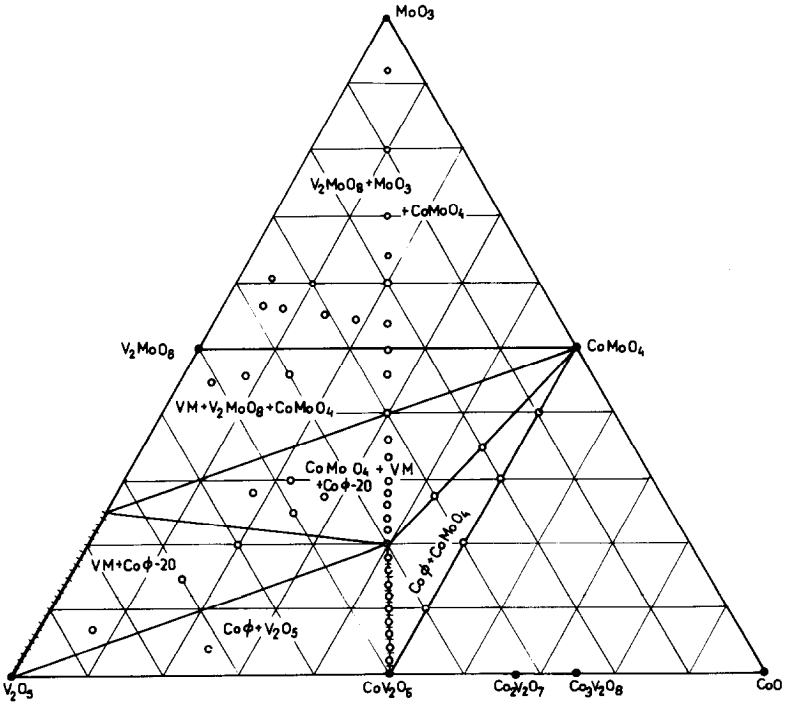

FIG. 3. Subsolidus portion of the phase diagram of the ternary CoO–V_2O_5–MoO_3 system divided into natural subdiagrams. Coϕ = $Co_{1-x}\phi_xV_{2-2x}Mo_2O_6$, *VM* = $V^{5+}_{2-2y}V^{4+}_yMo^{6+}_yO_5$; the lines along which these two solutions exist are dashed. The open points represent the composition of the studied samples.

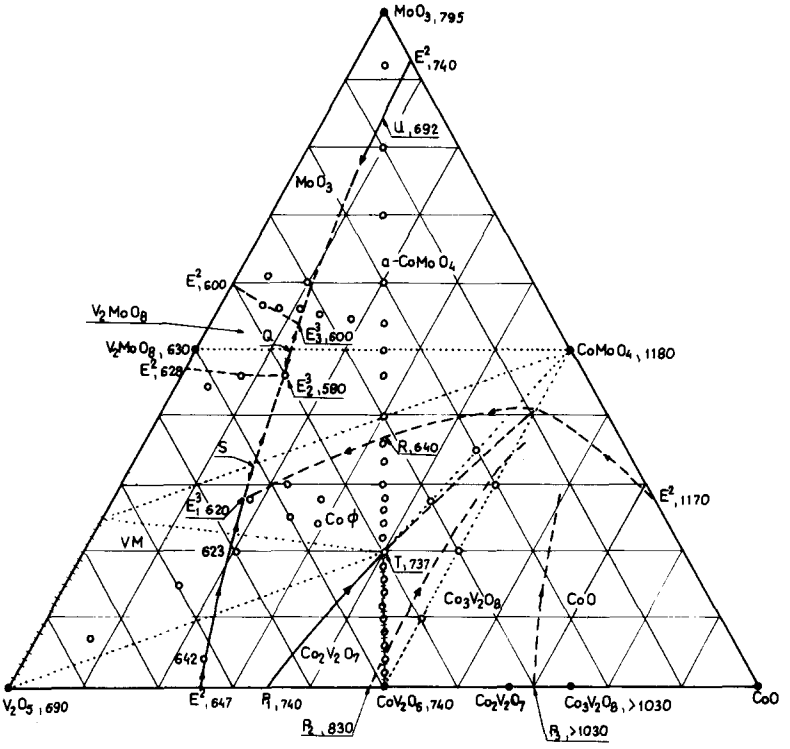

FIG. 4. Liquidus of the CoO–V_2O_5–MoO_3 system with marked: all binary compounds, their crystallization fields, binary (E^2) and ternary (E^3) eutectic and peritectic (P) points. Subsolidus (cf. Fig. 3) is recalled with pointed lines. The lines along which the Coϕ and *VM* solid solution exist are dashed. Capital letters mark the characteristic points to be compared with Fig. 5. The open points represent the composition of the studied samples.

$CoMoO_4$ (congruent m.p. 1180°C), and two binary eutectics, (7% CoO, 93% MoO_3, 740°C) and (72% CoO, 28% MoO_3, 1170°C) (all percentages in mole%). In view of our experiments the earlier data by Lipsch and Shuit (*19*) seem to be less accurate.

The T–CoO–V_2O_5 phase diagram has been determined by Brisi *et al.* (*14, 29*), partly reexamined by Clark and Pick (*16*) and verified in the present paper. There are three incongruently melting compounds in the system with peritectic points indicated in parentheses: CoV_2O_6 (34% CoO, 66% V_2O_5, 740°C), $Co_2V_2O_7$ (48% CoO, 52% V_2O_5, 830°C), $Co_3V_2O_8$ (70% CoO, 30% V_2O_5, above 1030°C). Moreover, there is one binary eutectic (25% CoO, 75% V_2O_5, 647°C).

The T–V_2O_5–MoO_3 diagram has been the subject of numerous studies (*30–34*) and it seems to be the most controversial one. According to our data, its most probable shape is the following: one congruently melting compound V_2MoO_8 (m.p. 630°C) which may form a solid solution with an excess of MoO_3 (*26*), two eutectics (40% V_2O_5, 60% MoO_3, 600°C), (53% V_2O_5, 47% MoO_3, 628°C) and a solid solution of MoO_3 in a V_2O_5 matrix with the solubility of about 25% MoO_3 at 628°C.

Basing on the DTA of the samples marked in Figs. 3 and 4, we have found that there are three ternary eutectics in the CoO–V_2O_5–MoO_3 system. These are: E_1^3 (18% CoO, 54% V_2O_5, 28% MoO_3, 620°C), E_2^3 (14% CoO, 40% V_2O_5, 46% MoO_3,

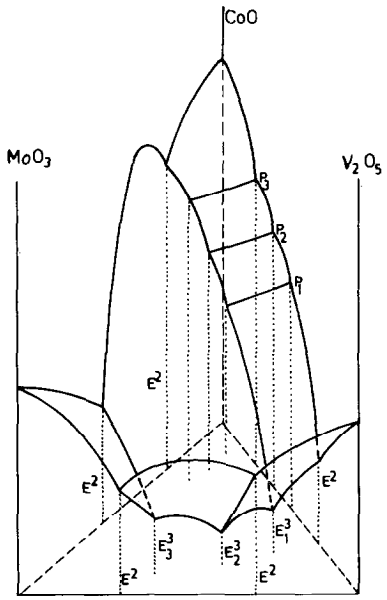

FIG. 5. An outline of liquidus of the $CoO–V_2O_5–MoO_3$ phase diagram.

580°C), E_3^3 (12% CoO, 34% V_2O_5, 54% MoO_3, 600°C). The error of composition is estimated to be 2–3% of each component. On this basis the liquidus part of the $T–CoO–V_2O_5–MoO_3$ diagram with indicated crystallization fields of MoO_3, V_2MoO_8, *VM*, $CoMoO_4$, α-Coϕ, $Co_2V_2O_7$, $Co_3V_2O_8$, and CoO has been constructed as shown in Figs. 4 and 5.

Selected samples of the $V_2O_5–MoO_3–CoMoO_4–CoV_2O_6$ field were partly melted at temperatures just above solidus (determined with DTA), slowly cooled (1,5°/hr) to about 20°C below solidus and submitted to the X-ray phase analysis. The expected composition was always confirmed.

Figure 6 shows the shape of the $T–CoV_2O_6–MoO_3$ slice consistent with Figs. 3 and 4. Solidus is determined here by three horizontal lines corresponding to the three ternary eutectics E_3^3 at 600°C, E_2^3 at 580°C,

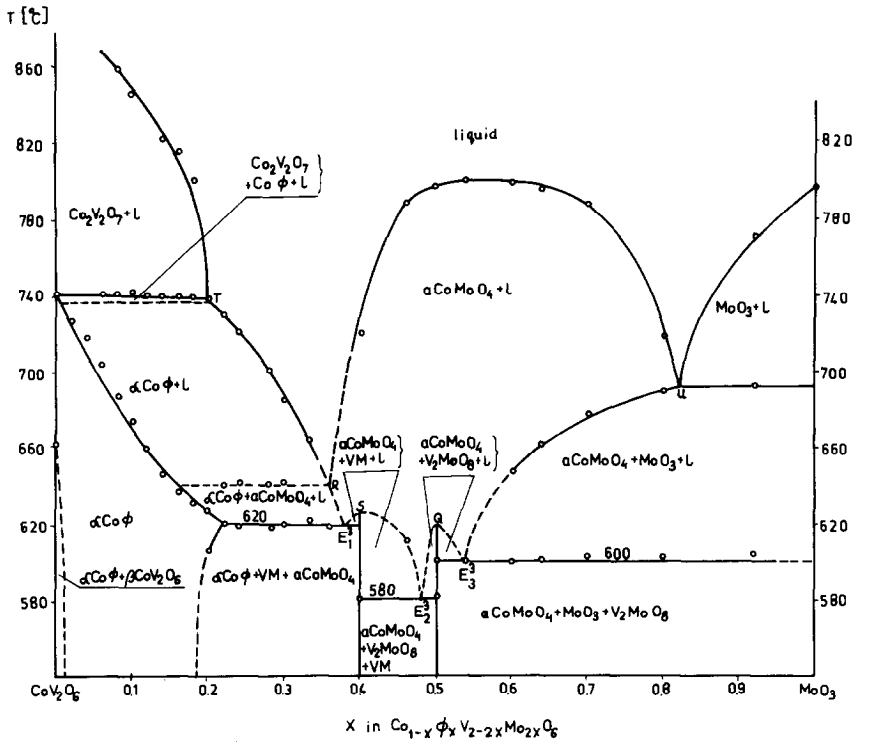

FIG. 6. The $T–CoV_2O_6–MoO_3$ slice of the $T–CoO–V_2O_5–MoO_3$ phase diagram. Capital letters mark the characteristic points to be compared with Fig. 4.

E_1^3 at 620°C and by a line climbing from (X = 22, 620°C) to (X = 0, 740°C), above which α-Coϕ begins to melt. Liquidus is determined by the respective sections through the crystallization surfaces of MoO_3, $CoMoO_4$, α-Coϕ, and $Co_2V_2O_7$. For easy comparison of Figs. 4 and 6 some characteristic points are marked with capital letters. All points and lines between liquidus and solidus in Fig. 6 are based on DTA, and an ascription of the fields to the coexistence of the respective phases is the logical consequence of the ternary diagrams presented in Figs. 3 and 4. The subsolidus range below $X = 3$ has already been discussed in paragraph (I). X_{max} of Coϕ-X is equal to 22 at the eutectic temperature of 620°C.

References

1. R. Kozłowski, J. Ziółkowski, K. Mocała, and J. Haber, *J. Solid State Chem.* **35,** 1 (1980); Erratum **38,** 138 (1981).
2. J. Ziółkowski, R. Kozłowski, K. Mocała, and J. Haber, *J. Solid State Chem.* **35,** 297 (1980).
3. T.Machej, R. Kozłowski, and J. Ziółkowski, *J. Solid State Chem.* **38,** 97 (1981).
4. R. Kozłowski and S. Stadnicka, *J. Solid State Chem.* **39,** 271 (1981).
5. J. Ziółkowski, K. Krupa, and K. Mocała, *J. Solid State Chem.* **48,** 376 (1983).
6. R. Ruh and A. D. Wadsley, *Acta Crystallogr.* **21,** 974 (1966).
7. H. N. Ng and C. Calvo, *Canad. J. Chem.* **50,** 3619 (1972).
8. J. Galy, J. Darriet, and B. Darriet, *C.R. Acad. Sci. Ser. C* **264,** 1477 (1967).
9. B. Darriet and J. Galy, *Bull. Soc. Fr. Mineral. Crystallogr.* **91,** 325 (1968).
10. J. Ziółkowski and J. Janas, *J. Catal.* **81,** 298 (1983).
11. J. Ziółkowski, *J. Catal.* **81,** 311 (1983).
12. J. Ziółkowski and M. Gasior, *J. Catal.* **84,** 74 (1983).
13. J. Ziółkowski, *J. Catal.* **84,** 317 (1983).
14. C. Brisi, *Ann. Chim.* **47,** 806 (1957).
15. E. E. Sauerbrei, M.S. thesis, McMaster University, Ontario, Canada (1972).
16. G. M. Clark and A. N. Pick, *J. Therm. Anal.* **7,** 289 (1975).
17. F. Y. Robb, W. S. Glaunsinger, and P. Courtine, *J. Solid State Chem.* **30,** 171 (1979).
18. P. Courtine and J. P. Daumas, *C.R. Acad., Sci. Paris* **268,** 1568 (1969).
19. J. H. J. G. Lipsch and G. C. A. Shuit, *J. Catal.* **15,** 163 (1969).
20. T. M. Yanushkevitch, V. M. Zhukovskii, and V. M. Ustyantsev, *Zh. Neorg. Khim.* **21,** 774 (1976).
21. P. Boutry, J. C. Daumas, R. Montarnal, P. Courtine, and P. Pannetier, *Bull. Soc. Chim. Fr.* 4811 (1968).
22. J. Haber, and J. Ziółkowski, *in* "Proceedings, 7th International Symposium on Reactivity of Solids" (Champan and Hall, Eds.), Bristol (1972).
23. J. Haber, J. Nowok, and J. Ziólkowski, *Bull. Acad. Pol. Sci. Ser. Sci. Chim.* **21,** 479 (1973).
24. J. Chojnacki, R. Kozłowski, and J. Haber, *J. Solid State Chem.* **11,** 106 (1974).
25. Joint Committee on Powder Diffraction Standards 1973, 9-387, 5-508, 21-868.
26. H. A. Eick and L. Kihloborg, *Acta Chim. Scand.* **20,** 1658 (1966).
27. R. D. Shannon and C. T. Prewitt, *Acta Crystallogr. Sect. B* **25,** 925 (1969).
28. R. D. Shannon, *Acta Crystallogr. Sect. A* **32,** 751 (1976).
29. V. Cirilli, A. Burdese, and C. Brisi, *Atti Accad. Sci. Torino* **95,** 1 (1960/61).
30. N. Strupler and A. Morett, *C.R. Acad. Sci. Paris* **260,** 1971 (1965).
31. N. Strupler and A. Morett, *Ann. Chim.* **10,** 345 (1965).
32. A. Bielański, K. Dyrek, J. Poźniczek, and E. Wenda, *Bull. Acad. Pol. Sci., Ser. Sci. Chim.* **19,** 507 (1971).
33. A. bielański and J. Najbar, *Pol. J. Chem.* **52,** 883 (1978).
34. V. L. Volkov, G. S. Tynkatscheva, A. A. Fotiev, and E. V. Tkatschenko, *Zh. Neorg. Khim.* **17,** 2803 (1972).